循環器における小胞体タンパク質

TRIC に関する研究

2013

陶　晟辰

The Research on TRIC Channels

in Cardiovascular Systems

Introductions……1

Experimental Procedures……4

Results……8

Discussion……27

Summary……33

Acknowledgment……34

Publication List……35

References……36

The abbreviations used are as follows:

BK channel, big-conductance Ca^{2+}-dependent K^+ channel;

$[Ca^{2+}]_i$, intracellular Ca^{2+} concentration;

CICR, Ca^{2+}-induced Ca^{2+} release;

CPA, cyclopiazonic acid;

ER, endoplasmic reticulum;

HBS, HEPES-buffered saline;

IBTX, iberiotoxin;

IP_3R, inositol 1,4,5-trisphosphate receptors;

PE, phenylephrine;

RyR, ryanodine receptor;

SOCE, store-operated Ca^{2+} entry;

STOC, spontaneous transient outward current;

SR, sarcoplasmic reticulum;

TRIC, trimeric intracellular cation;

VSMC, vascular smooth muscle cell.

Introductions

Two major classes of intracellular Ca^{2+} channels, inositol 1,4,5-trisphosphate receptors (IP_3Rs) and ryanodine receptors (RyRs), provide the fundamental pathway for Ca^{2+} release from internal stores into the cytoplasm (1-4). IP_3R-mediated Ca^{2+} release from IP_3-sensitive stores in the sarco/endoplasmic reticulum (SR/ER) plays a central role in cellular signaling systems. RyR-mediated Ca^{2+} release from caffeine-sensitive stores also regulates important cellular functions, such as excitation-contraction coupling, secretion/exocytosis and gene expression, primarily in excitable cells. When the divalent cation Ca^{2+} is released from the SR/ER, a negative potential is likely generated on the luminal side and may inhibit subsequent Ca^{2+} release. Therefore, counter-ion movements may balance SR/ER membrane potential to establish efficient Ca^{2+} release mechanisms in various cell types (5, 6). Indeed, previous electrophysiological and fluorometric analyses detected several ionic currents, such as K^+, Cl^- and H^+ fluxes, across the SR/ER membrane (7-10). However, the channel/transporter components mediating such ionic flows have not been identified, and thus, their contributions to the proposed counter-ion movements are largely unknown.

Recently, we identified two TRIC (trimeric intracellular cation) channel subtypes, TRIC-A and TRIC-B, which assemble into bullet-shaped homo-trimers to form monovalent cation-selective channels in the SR/ER and nuclear membranes, (11-13, Table 1). Double-knockout mice lacking both the *Tric-a* and *Tric-b* genes show

embryonic cardiac failure, and the mutant cardiomyocytes display weak RyR-mediated Ca^{2+} release from the SR (14). *Tric-a*-knockout mice develop hypertension associated with vascular hypertonicity, and the mutant vascular smooth muscle cells (VSMCs) show insufficient Ca^{2+} sparks for inducing hyperpolarization (15). Moreover, mutant skeletal muscle from *Tric-a*-knockout mice occasionally exhibits alternan contraction responses, likely due to destabilized RyR-mediated Ca^{2+} release (16). On the other hand, *Tric-b*-knockout mice develop respiratory failure at birth, and the mutant alveolar epithelial cells exhibit compromised IP_3R-mediated Ca^{2+} release and insufficient handling of surfactant lipids (17). These defects observed in the knockout mice support our hypothesis that TRIC channel subtypes partly mediate counter-ion movements to facilitate SR/ER Ca^{2+} release (Fig. 1).

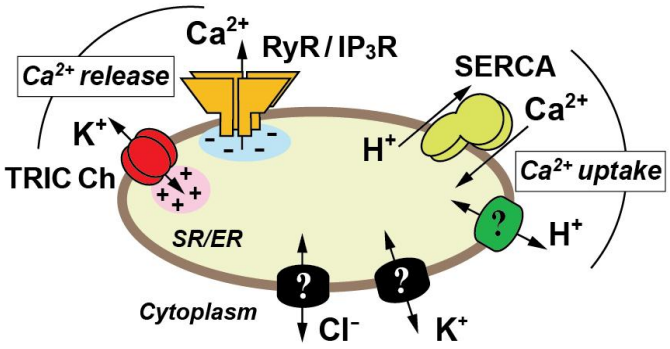

Figure 1. Proposed role of TRIC channels in Ca^{2+} handling of intracellular stores.
Physiological Ca^{2+} release mediated by RyR and IP_3R channels probably requires counter-ion movement to neutralize the accumulation of transient negative potential across the SR/ER. Several H^+, K^+ or Cl^- selective channels were proposed on the ER/SR from electrophysiological and biochemical data, but their molecular identities and biological functions remain to be elucidated.

Table 1. TRIC channels in mice.

Mouse	TRIC-A	TRIC-B
Chromosome	8B3.3	4B2
Amino acid	298 aa	292 aa
Homology	39.1% (mouse)	
Expression tissue	Excitable tissue (Nervous, Cardiac muscle, Seletal muscle)	Ubiquitous
Subcellular localization	Nuclear membrane, ER/SR membrane	ER/SR membrane
Topology	3 TM domain	3 TM domain ?
Oligomer	Trimer	
Channel activity	Present	
Ion selectivity	K^+>Na^+ (1.5:1)	?
TRIC-A(-/-)B(+/-)	Ca^{2+} overload in SR of skeletal muscle	
TRIC-A(-/-)B(-/-)	Embryonic lethal at E9.5	
KO mice phenotype	Alternan contraction Hypertension	Neonatal lethal

VSMCs possess both caffeine- and IP_3-sensitive stores and also contain both TRIC-A and TRIC-B channels (Fig. 2). Therefore, VSMCs are an ideal model system to examine the physiological functions of TRIC channel subtypes. Our research group recently detected not only insufficient RyR-mediated Ca^{2+} sparks but also facilitated IP_3R-mediated Ca^{2+} transients in *Tric-a*-knockout VSMCs (15). These observations led to the hypothesis that TRIC-A channels preferentially support RyR-mediated Ca^{2+} release and also regulate Ca^{2+} distribution between the caffeine- and IP_3-sensitive stores. To further verify this hypothesis, I planned to generate mutant mice carrying the SMC-specific *Tric-a* transgene and to examine altered features in *Tric-a*-overexpressing VSMCs

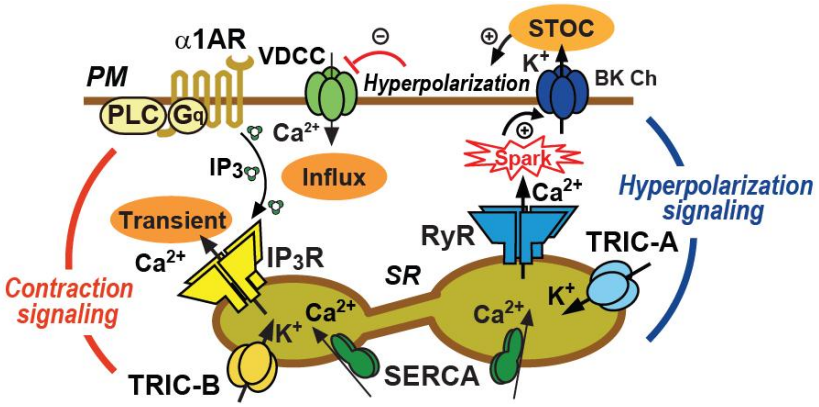

Figure 2. Contraction signaling and hyperpolarization signaling in VSMCs

Experimental Procedures

Transgenic Mice and Blood Pressure Monitoring

Transgenic mice overexpressing TRIC-A channels under the control of the human α-smooth muscle actin promoter were generated and genotyped as previously described (15, Fig. 3). The transgenic and wild-type littermates (8-12 weeks old) were examined physiologically and biochemically in this study. All experiments were conducted with the approval of the Animal Research Committee at Kyoto University according to the regulations on animal experimentation at Kyoto University. To telemetrically monitor arterial blood pressure, PA-C10 transmitters (Data Sciences International, New Brighton, MN, US) were implanted into mice, and the pressure-sensing catheters were inserted

into the aortic arch under anesthesia. Radio signals from the implanted transmitter were captured using the Physiotel RPC-1 receiver (Data Sciences International), and the data were stored online using the Dataquest ART data acquisition system (Data Sciences International). Blood pressure and heart rate in the conscious state were also monitored by tail-cuff plethysmography (Model BP-98A-L, Softron, Japan) during the daytime.

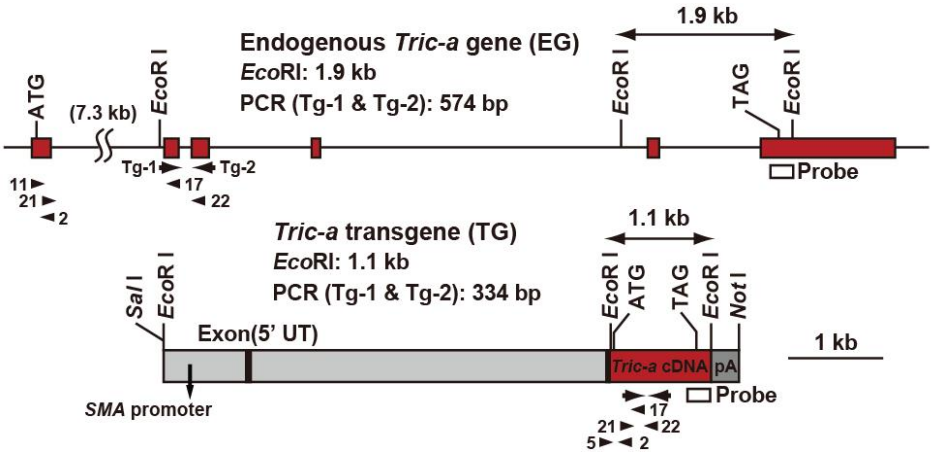

Figure 3. The production and confirmation of *Tric-a* transgene mice

Maps of the endogenous *Tric-a* gene (EG) and the SMC-specific *Tric-a* transgene (TG). Synthetic primers for PCR analysis are indicated by arrows (for mouse genotyping) and arrowheads (for RT-PCR analysis). A hybridization probe used for Southern blot analysis of *Eco*RI-digested genomic DNAs is indicated by an open box. Transcriptional regions are marked by red boxes.

Anatomical Analysis

Histological and ultrastructural analyses were carried out as described previously (18). Briefly, mesenteric arteries from adult mice were fixed in 3% paraformaldehyde, 2.5% glutaraldehyde and 0.1 M sodium cacodylate (pH 7.4). After the tissues were dehydrated and embedded in Epon, ultrathin sections (~80-nm thick) were prepared and

stained with toluidine blue for histological observation or uranyl acetate and lead citrate for electron-microscopic analysis (JEM-200CX, JEOL).

Imaging Analysis

Single VSMCs were enzymatically isolated from mesenteric arteries and subjected to Ca^{2+} spark and membrane potential monitoring as described previously (15, 19). Briefly, single VSMCs were seeded onto glass-bottomed dishes and incubated with 5 μM Fluo-4AM (Dojindo, Japan) in HEPES-buffered saline (HBS, in mM: 137 NaCl, 5.9 KCl, 2.2 $CaCl_2$, 1.2 $MgCl_2$, 14 glucose and 10 HEPES, pH 7.4 with NaOH). The Ca^{2+} spark images with excitation at 488 nm and emission at >520 nm were captured using a total internal reflection fluorescence microscopy system (TE-2000U, Nikon), and the data were analyzed using the custom software Aquacosmos (Hamamatsu Photonics). For membrane potential monitoring, single VSMCs on glass-bottomed dishes were perfused with HBS containing 200 nM oxonol VI (Fluka). Fluorescence images with excitation at 559 nm and emission at >606 nm were captured at a sampling rate of ~1.6 s using a confocal microscope system (FV1000, Olympus).

For monitoring intracellular Ca^{2+} concentration ($[Ca^{2+}]_i$) in VSMCs, the inner surface of the artery was gently wiped with gauze to remove endothelial cells as described previously (20). The resulting arterial muscle segments were incubated with 5 μM Fura-PE3AM (Santa Cruz) and 0.02% cremophor EL (Sigma-Aldrich) and tightly fixed with fine steel pins onto a silicone rubber sheet, which was placed on a glass-bottomed dish. A CCD camera (ImagEM, Hamamatsu Photonics) mounted on the

microscope (DMI 4000B, Leica) equipped with a polychromatic illumination system (MetaFluor ver7.7r3, Molecular Device) was used to capture fluorescence images with excitation at 340 and 380 nm and emission at >510 nm at room temperature (~23 ºC).

Patch-Clamp and Membrane Potential Recording

Whole-cell voltage-clamp recording was carried out using the Axopatch 200B amplifier (Molecular Device) essentially as described previously (21). For spontaneous transient outward current (STOC) monitoring in single VSMCs, the STOC pipette solution (in mM: 140 KCl, 4 $MgCl_2$, 5 Na_2ATP, 0.05 EGTA and 10 HEPES, pH 7.2 with KOH) and HBS as a bathing solution were utilized. For the recording of total Ca^{2+}-dependent K^+ currents, the BK pipette solution (in mM: 140 KCl, 1 $MgCl_2$, 6.1 $CaCl_2$, 1 Na_2ATP, 10 EGTA and 10 HEPES, pH 7.2 with KOH, pCa 6.5) and HBS containing 100 μM $CdCl_2$ as a bathing solution were utilized. All physiological measurements were carried out at room temperature.

The arterial muscle segments were subjected to transmembrane potential monitoring with high-resistance glass microelectrodes (30–50 MΩ) filled with 3 M KCl solution as described previously (22). Membrane potential was determined as an average of the potentials obtained from stable impalements longer than 1 min from different areas in the muscle segment. The transmembrane potential was amplified by a high-input impedance amplifier with capacitance neutralization (MEZ-7200, Nihon Kohden, Japan), and the electrical signals were digitized and analyzed using a Power Lab system (AD Instruments, New Zealand). The bath solution used was modified Krebs solution

babbled with 95% O_2-5% CO_2 and maintained at 37 ºC at pH ~7.4 (in mM: 112 NaCl, 4.7 KCl, 2.2 $CaCl_2$, 1.2 $MgSO_4$, 25 $NaHCO_3$, 1.2 KH_2PO_4, and 14 glucose).

RT-PCR and Immunochemical Analysis

For quantitative PCR analysis, total RNA preparations from various tissues (at least three mice of each genotype) were used as templates for cDNA synthesis (ReverTra ACE qPCR-RT kit, Toyobo, Japan) and analyzed using a real-time PCR system according to the manufacturer's instructions (Thermal Cycler TP800, Takara, Japan). The cycle threshold was determined from the cDNA amplification curve as an index for relative mRNA content in each reaction. The PCR primer sets used in this study were listed previously (15). For immunochemical analysis, tissue lysates and fixed VSMCs were examined using primary antibodies to TRIC channel subtypes and calnexin (Santa Cruz) as described previously (14, 18).

Results

Hypotension in SMC-Specific *Tric-a*-Transgenic Mice

We previously generated transgenic mice with SMC-specific overexpression of TRIC-A channels using the α-smooth muscle actin promoter (23). Although the constructed *Tric-a*-transgene rescues the hypertensive phenotype developed in *Tric-a*-knockout mice

(15), the effects of the transgene have not been examined in a wild-type genetic background. Therefore, our research group generated two *Tric-a*-transgenic mouse lines in wild-type backgrounds, which our research group designated as TgA3 and TgA20 mice. Both transgenic mouse lines grew and reproduced normally (Fig. 4A). RT-PCR analysis demonstrated that the transgene was highly expressed in blood vessels and other tissues containing SMCs, and its expression was faintly detected in the liver and skeletal muscle (Fig. 4B). In accordance with our previous observation that the transgene dosage in the TgA20 mouse line is higher than in the TgA3 line (15), TgA20 mice showed higher transgene expression in SMC-containing tissues than TgA3 mice in RT-PCR analysis (Fig. 4C).

By telemetric blood pressure monitoring, both TgA20 and TgA3 mice, even at a young-adult age, showed low blood pressure levels throughout the entire day (Fig. 5A).This hypotensive phenotype was further confirmed by tail-cuff monitoring (Fig. 5B). Most likely reflecting the difference in transgene expression between the mouse lines, TgA20 mice developed slightly lower blood pressure than TgA3 mice. Elevated blood pressure stimulates the baroreceptor reflex and effectively decreases heart rate in normal animals (24). However, in both transgenic mice, a slow heart rate was clearly observed under hypotensive conditions. The blockage of cardiac autonomic controls by coapplication of the muscarinic blocker atropine and the β-adrenoceptor blocker metoprolol ameliorated the bradycardic phenotype, whereas low blood pressure was clearly maintained in the transgenic mice (Fig. 5B). Therefore, ectopic *Tric-a* expression in baroreceptors and/or autonomic neurons likely produced vagal-dominant states in

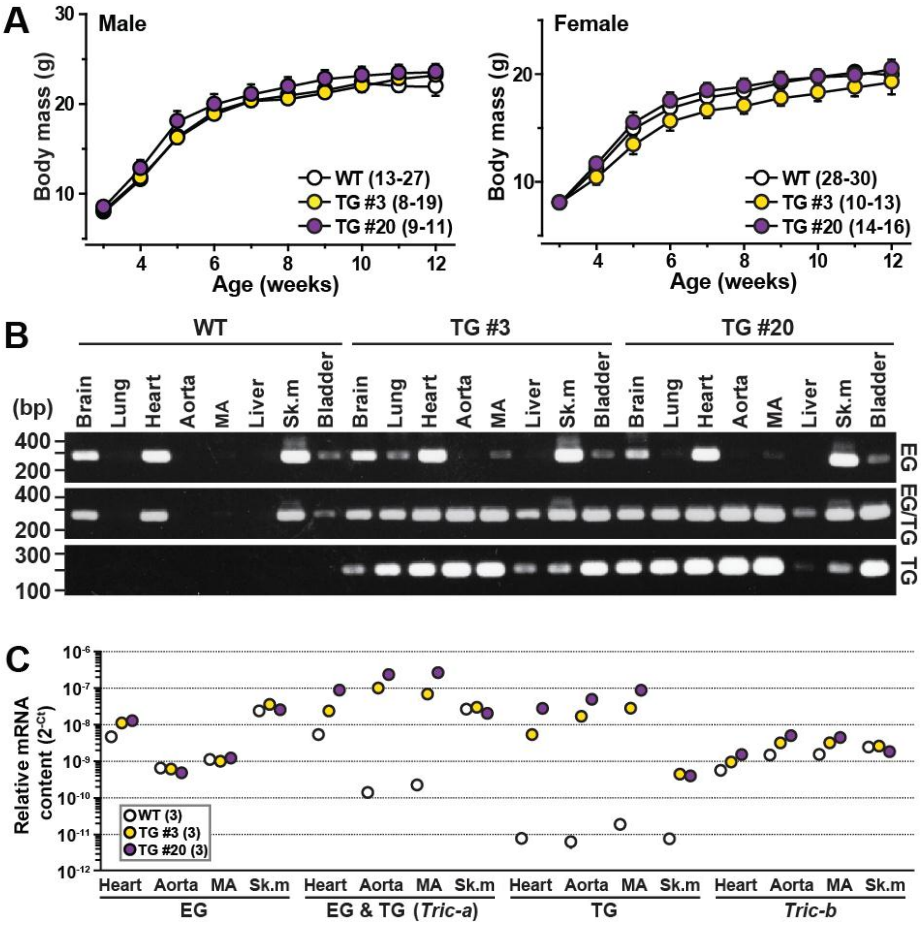

Figure 4. Postnatal growth, *Tric-a* gene expression and blood pressure responses in SMC-specific *Tric-a*-transgenic mice.

(*A*) Changes body weight of the *Tric-a*-transgenic mice and wild-type littermates. No significant difference was observed between the genotypes. (*B*) RT-PCR detection of *Tric-a* mRNA derived from the endogenous gene (EG) and the transgene (TG). Total tissue RNA preparations from at least three mice of each genotype were examined by quantitative RT-PCR analysis, and amplified cDNAs were analyzed on agarose gel electrophoresis. Expression of *Tric-b* mRNA was also examined in parallel (data not shown). (*C*) Relative expression of *Tric-a* and *Tric-b* mRNAs in tissues from the *Tric-a*-transgenic mice. The cycle threshold (Ct) was determined from the cDNA amplification curve as an index for relative mRNA content in each reaction.

both transgenic mice. Moreover, the α1-adrenoceptor blocker prazosin induced similar vasodilating effects in both wild-type and transgenic mice (Fig. 5C). These observations suggest that impaired sympathetic stimuli to the heart and vascular smooth muscle were not significant contributors to hypotension in the transgenic mice. It may be reasonable that altered vascular functions underlie the hypotensive phenotype in both transgenic mice because *Tric-a*-knockout mice develop hypertension due to increased vascular tonus (15).

Tric-a-Overexpressing VSMCs from the Transgenic Mice

Resistance arteries distributed to peripheral tissues are primarily responsible for blood pressure maintenance. The mesenteric artery is a typical resistance vessel and was examined in our studies below. By RT-PCR analysis of mesenteric arteries, the *Tric-a* mRNA levels in TgA20 and TgA3 mice were at least 400-fold greater than those of wild-type controls (Fig. 6A). Western blot analysis confirmed *Tric-a* overexpression, and enhanced immunoreactivities provided estimates that the TRIC-A protein levels in the arteries from the transgenic mice were increased more than 500-fold compared with wild-type arteries (Fig. 6B). However, neither the heart nor skeletal muscle from the transgenic mice showed an obvious enhancement of TRIC-A immunoreactivity (Fig. 6C). Such SMC-specific overexpression of TRIC-A channels may not cause serious damage to the fundamental functions of resistance arteries because the transgenic mice retained circadian blood pressure variation (Fig. 5A) and regular blood pressure fluctuation in response to typical vasodilators targeting VSMCs (Fig. 5C).

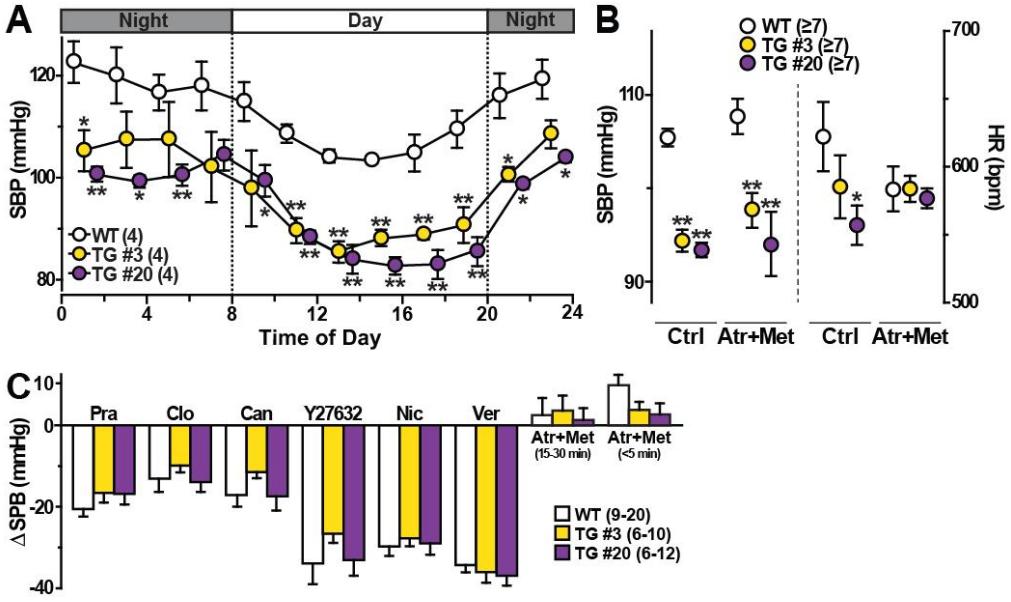

Figure 5. Hypotension in SMC-specific *Tric-a*-transgenic mice.

(*A*) Telemetric blood pressure monitoring. Circadian fluctuations in systolic blood pressure (SBP) were monitored, and the data were averaged over each 2-hr interval during a 24-hr period. (*B*) SBP and heart rate (HR) monitoring by tail-cuff plethysmography during the daytime. After the baseline monitoring (Ctrl), autonomic controls were blocked using an intraperitoneal injection of the muscarinic antagonist atropine (Atr, 4 mg/kg) and the β-antagonist metoprolol (Met, 4 mg/kg). Upon drug application, HR was quickly attenuated, but SBP changed in a time-dependent manner (*C*). (*C*) Pharmacological effects of various agents on systolic blood pressure monitored by tail-cuff plethysmography in the *Tric-a*-transgenic and wild-type mice during daylight hours. Drugs used for analysis were the α1-antagonist prazosin (Pra, 1 mg/kg), α2-agonist clonidine (Clo, 0.1 mg/kg), angiotensin II AT1-receptor blocker candesartan (Can, 10 mg/kg), Rho kinase inhibitor Y27632 (5 mg/kg), dihydropyridine Ca^{2+} antagonist nicardipine (Nic, 1 mg/kg), phenylalkylamine Ca^{2+} antagonist verapamil (Ver, 12 mg/kg), muscarinic antagonist atropine (Atr, 4 mg/kg) and β1-antagonist metoprolol (Met, 4 mg/kg). The effects of autonomic blockage with atropine and metoprolol were slightly time-dependent, and the data at approximately 5 min and 15-30 min after drug injection are presented. The data represent the mean ± SEM, and the numbers of mice examined are shown in parentheses. Significant differences between the genotypes are indicated by asterisks (*****p<0.05, ******p<0.01 by *t*-test).

Histological observations revealed no obvious abnormalities in mesenteric arteries from TgA20 and TgA3 mice (Fig. 7A). For example, under relaxation conditions after incubation in a Ca^{2+}-free bathing solution, similar passive diameters and VSMC layer thicknesses of the arteries were observed in the transgenic and wild-type mice (Fig. 7A). These observations suggest that the hypotensive phenotype was mainly caused by insufficient myogenic tonus of resistance arteries under *in vivo* conditions in the transgenic mice.

Electron microscopic observation detected irregular membranous ultrastructure in mesenteric arteries from the transgenic mice. In *Tric-a*-overexpressing VSMCs, stacked rough ER elements accumulated around cell-interior regions (Fig. 7B, left panels). The generation of stacked rough ER has been repeatedly reported in various cell types overexpressing integral SR/ER membrane proteins (25, 26), and such irregular ER elements were not detected in wild-type VSMCs. Indeed, dense immunofluorescence signals of ectopic TRIC-A channels were predominantly observed in the cell-interior regions of VSMCs from transgenic mice (Fig. 8B), suggesting that the ER stacks were generated by nonspecific effects of excess TRIC-A protein. In SMCs, IP_3Rs are distributed uniformly over the nuclear and ER/SR membranes (27, 28), whereas RyRs are predominantly localized in peripheral SR elements (29, 30). Therefore, it is possible that the formation of the stacked rough ER may have a functional impact on IP_3-sensitive stores. However, such a morphological abnormality may minimally affect caffeine-sensitive stores.

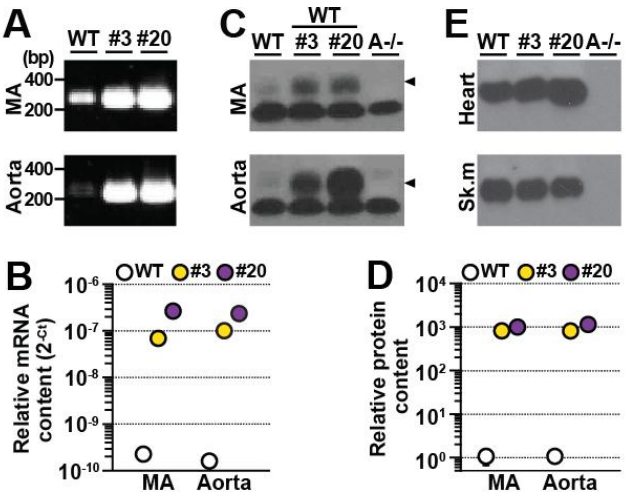

Figure 6. Irregular membranous features of *Tric-a*-overexpressing VSMCs.

(*A*) Quantitative detection of *Tric-a* mRNA in mesenteric artery (MA) and aorta. Total tissue RNA preparations from transgenic (#3 and #20) and wild-type mice (n=3) were examined by quantitative RT-PCR using a primer set for amplifying *Tric-a* mRNA from both the endogenous gene and the transgene. The cDNA fragments amplified by 33 PCR cycles were analyzed by agarose gel electrophoresis. RT-PCR data obtained are summarized in the (*B*). The cycle threshold (Ct) indicates the cycle number at which the amount of amplified cDNA reached a fixed threshold in each reaction. (*C*) Western blot analysis of TRIC-A protein in MA and aorta. The vessels dissected from the *Tric-a*-transgenic (#3 and #20), *Tric-a*-knockout (A-/-) and wild-type mice were homogenized to prepare total cell lysates (post-nuclear fractions). Wild-type lysates (10 μg protein), with or without lysates from the transgenic mice (0.1 μg), were analyzed with an antibody against the TRIC-A protein. Lysates from the *Tric-a*-knockout mice (10 μg) served as negative controls. Arrowheads indicate TRIC-A protein bands. Immunoreactive signals were digitalized and statistically analyzed to estimate the relative contents of TRIC-A protein in the different genotypes as shown in the (*D*). (*E*) Normal TRIC-A protein levels in the heart and skeletal muscle from the *Tric-a*-transgenic mice. Postnuclear lysates (2 and 0.5 μg protein for heart and skeletal muscle, respectively) from the *Tric-a*-transgenic, *Tric-a*-knockout and wild-type mice were analyzed by Western blotting using an antibody against the TRIC-A protein. Although RT-PCR detected transgene expression in striated muscle, TRIC-A protein levels were not significantly elevated in the heart or skeletal muscle.

In VSMCs, free-floating small vesicles, originally referred to as “surface vesicles” (31), were abundantly arranged underneath the cell membrane (Fig. 7B, right panels). Accompanied by the surface vesicles, larger-sized vacuoles with myelin figures (multilamellar lipid deposits) or without electron-dense material in the lumen were frequently observed in *Tric-a*-overexpressing VSMCs. Such vacuoles were rarely detected in wild-type VSMCs. In order to resolve the stacked ER elements, the large vacuoles may be aberrantly generated in *Tric-a*-overexpressing VSMCs. Alternatively, the excess amounts of TRIC-A protein may have promoted the swelling and fusion of normal small vesicles, generating the vacuoles. Swelling of SR elements is frequently accompanied by stored Ca^{2+} overloading in skeletal and cardiac muscle (16, 32, 33), and RyR-mediated Ca^{2+} sparks are predominantly generated underneath the cell membrane in VSMCs (3, 4). The facilitated formation of the vacuoles may imply altered Ca^{2+}-handling characteristics in caffeine-sensitive stores of *Tric-a*-overexpressing VSMCs.

Facilitated Hyperpolarization Signaling in *Tric-a*-Overexpressing VSMCs

In VSMCs, incidental activation of RyRs generates Ca^{2+} sparks and then activates big-conductance Ca^{2+}-dependent K^+ (BK) channels to evoke STOCs, leading to hyperpolarization (3, 4). To identify the direct cause of the hypotensive phenotype, Our research group investigated Ca^{2+} spark and STOC generation in VSMCs from the transgenic mice because hyperpolarization signaling is impaired in *Tric-a*-knockout VSMCs (15). Our Ca^{2+} spark imaging captured hyperactivated sparks at specified

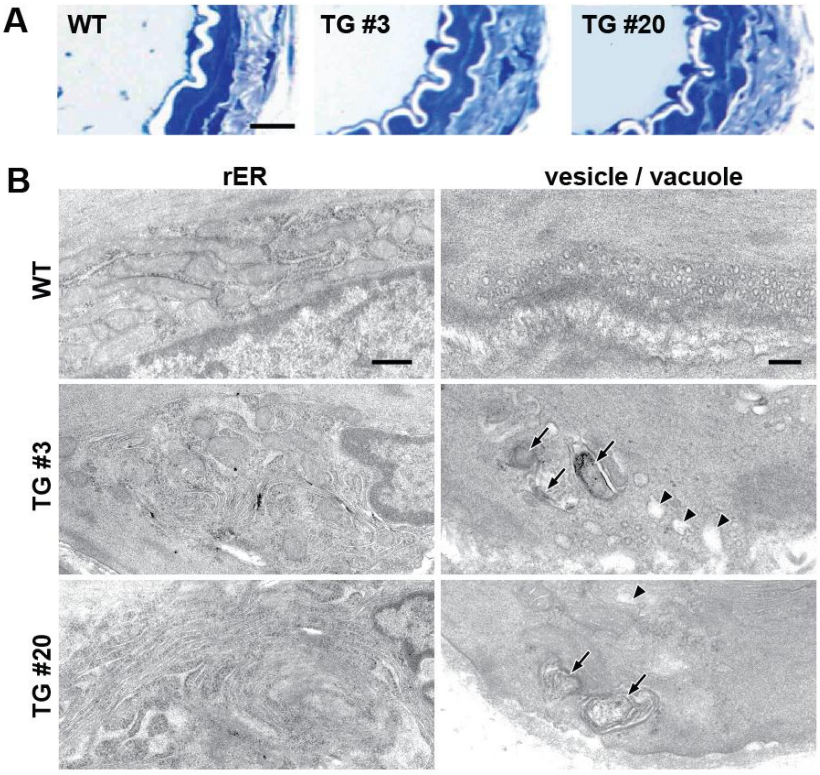

Figure 7. Irregular membranous features of *Tric-a*-overexpressing VSMCs.

(*A*) Normal histology in MA from *Tric-a*-transgenic mice. MA preparations were incubated in a Ca^{2+}-free solution for ~20 min and then fixed for anatomical analysis. Thin sections were stained with toluidine blue for photomicroscopic observation. *IVL*, intravascular lumen. Scale bar, 10 μm. (*B*) Formation of stacked ER elements and vacuoles in *Tric-a*-overexpressing VSMCs. Rough ER elements at the cell-interior portion (left panels: scale bar, 500 nm). Stacks of rough ER elements were frequently observed in VSMCs from transgenic mice (approximately 27% of TgA3 cells and 80% of TgA20 cells), whereas such stacked ER was not detected in wild-type controls (n = 45-97 cells from 3-6 mice in each genotype). Surface vesicles and vacuoles were located at the cell periphery (right panels: scale bar, 200 nm). TRIC-A overexpression appeared to promote the formation of large-sized vacuoles containing myelin figures (arrows) or no electron-dense materials (arrowheads). Such vacuoles were frequently observed in more than 50% of VSMCs from TgA3 and TgA20 mice, but only detected in 9.5% of wild-type VSMCs (n = 53-89 cells from 6 mice in each genotype).

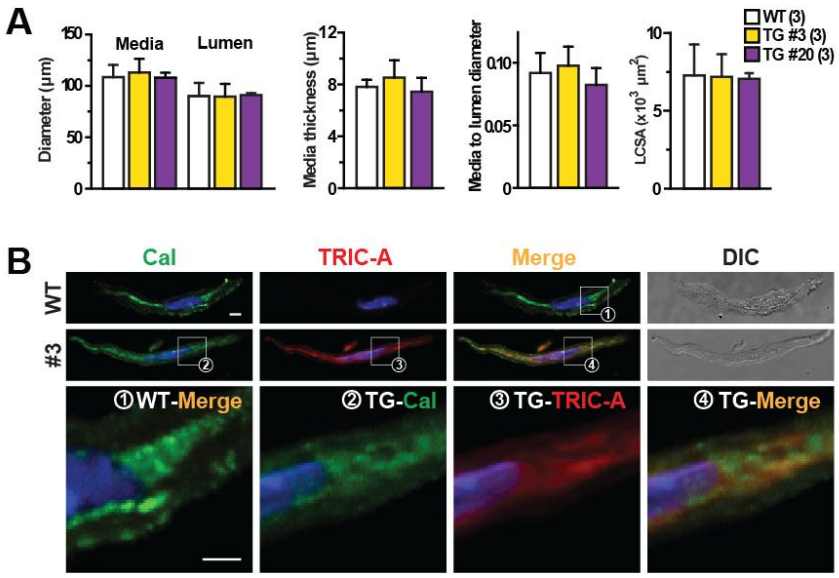

Figure 8. Histological analysis of mesenteric arteries from SMC-specific *Tric-a*-transgenic mice.

(*A*) Normal histological parameters of mesenteric arteries from *Tric-a*-transgenic mice. After incubation in a Ca^{2+}-free solution, relaxed mesenteric arteries were fixed for anatomical analysis and observed with a photomicroscope. We analyzed the media diameter, lumen diameter, media thickness, media to lumen diameter and lumen cross-sectional area (LCSA) of the arterial sections from three mice using Image J software. No significant difference was detected between the genotypes in each analysis. (*B*) Immunocytochemical detection of TRIC-A protein in *Tric-a*-overexpressing VSMCs. *Tric-a*-overexpressing and wild-type VSMCs were immunostained using antibodies to TRIC-A protein and the ER marker calnexin and examined using a confocal microscope. No immunostaining with anti-TRIC-A antibody was detected in wild-type VSMCs (upper row), but dense immunostaining was observed at perinuclear regions in *Tric-a*-overexpressing VSMCs from TgA3 mice (middle row). VSMC images using a differential interference contrast (DIC) microscope are also presented. Numbered inset regions are also shown at high magnification (lower row). Scale bars, 2 μm.

intracellular hotspots in single VSMCs prepared from the transgenic mice (Fig. 9A). Statistical analysis of the imaging data detected no difference in Ca^{2+} spark amplitude between the genotypes. However, Ca^{2+} spark frequency was substantially elevated and the number of spark hotspots was significantly increased in *Tric-a*-overexpressing VSMCs from both TgA20 and TgA3 mice (Fig. 9B-D). RT-PCR analysis detected no altered gene expression of the key components in intracellular Ca^{2+} signaling and G protein-coupled receptor signaling, such as RyR, IP_3R, Ca^{2+}-pump protein, α-adrenoceptor and phospholipase C, in mesenteric arteries and thoracic aorta from the transgenic mice (Fig. 10). Therefore, *Tric-a* overexpression appears to hyperactivate Ca^{2+} spark generation without affecting the cellular levels of major Ca^{2+}-handling proteins in VSMCs.

For monitoring BK channel-mediated STOCs, single VSMCs were examined by patch-clamp recording using the nominally Ca^{2+}-free STOC pipette solution. VSMCs from the transgenic mice showed highly activated STOCs (Fig. 11A). In particular, both STOC frequency and amplitude were markedly increased at a holding potential of -60 mV near the resting potential in the *Tric-a*-overexpressing cells (Fig. 11B). which our research group also monitored total K^+ currents using the Ca^{2+}-containing BK pipette solution and examined the effects of the BK channel inhibitor iberiotoxin on VSMCs. VSMCs from the transgenic mice showed normal levels of total K^+ currents both sensitive and insensitive to iberiotoxin (Fig. 12). Therefore, despite normal cell-surface densities of BK channels, STOC generation was likely facilitated under physiological conditions in *Tric-a*-overexpressing VSMCs. The enhanced STOCs were fully

consistent with the hyperactivated Ca^{2+} sparks observed (Fig. 9), suggesting that hyperpolarization signaling generated by functional crosstalk between the RyR and BK channels was stimulated in VSMCs from the transgenic mice.

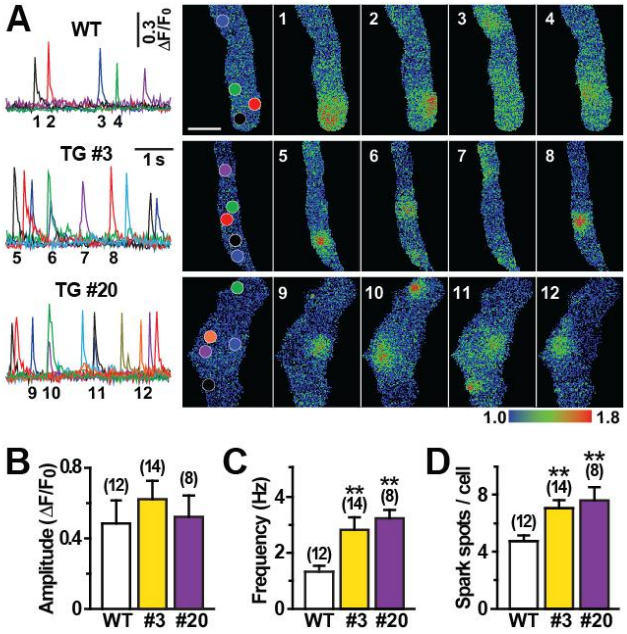

Figure 9. Facilitated Ca^{2+} sparks in *Tric-a*-overexpressing VSMCs.

Single VSMCs were prepared from mesenteric arteries and loaded with Fluo-4 for total internal reflection fluorescence imaging. (*A*) Representative Ca^{2+}-spark monitoring data in a normal bathing solution. The fluorescence intensity was normalized to the baseline intensity to yield the relative intensity (F/F_0), and time courses of the intensity changes at the subcellular hotspots (see colored circles in the F_0 cell images) are illustrated in the traces (scale bar, 5 μm). The F/F_0 images were color coded as indicated by the bar to prepare the Ca^{2+}-spark images at the numbered time points. The data on spark amplitude (*B*), frequency (*C*) and spot number (*D*) are summarized for each genotype. Significant differences between the genotypes are indicated by asterisks (**p<0.01 by *t*-test).

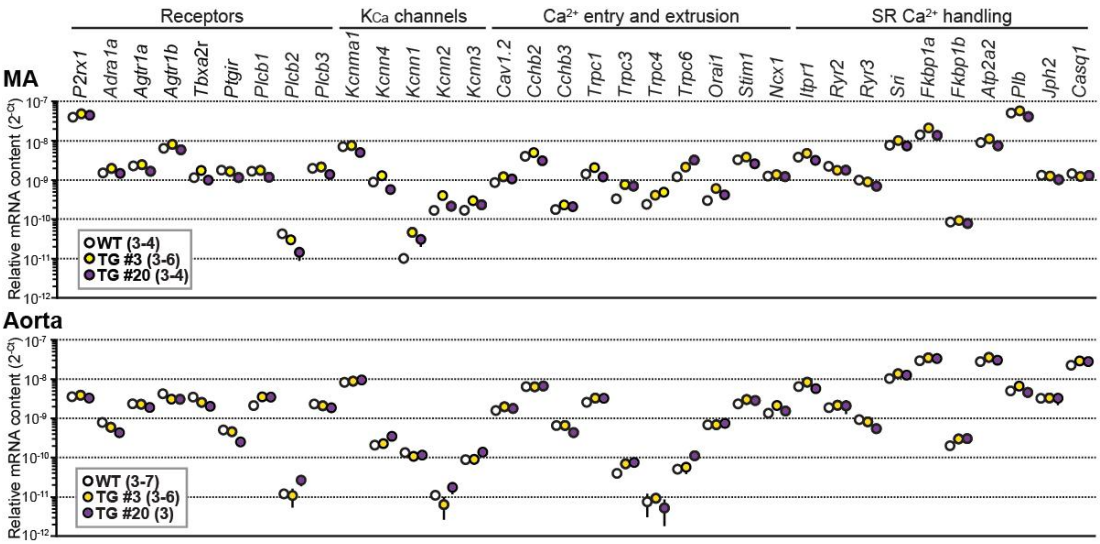

Figure 10. Signaling proteins in *Tric-a*-overexpressing VSMCs.

Quantitative RT-PCR analysis in mesenteric artery (MA) and thoracic aorta. The cycle threshold (Ct) was determined from the cDNA amplification curve as an index for relative mRNA content. For the data presentation, the mRNAs examined are tentatively categorized into four groups. Statistical evaluation detected no significant differences between the genotypes.

Deepened Resting Potential in *Tric-a*-Overexpressing VSMCs

In SMCs, BK channel-mediated STOCs contribute to the maintenance of resting membrane potential and the fine-tuning of cellular excitability (3, 4). Based on the facilitated STOCs observed, I next focused on membrane potential in *Tric-a*-overexpressing VSMCs and leveraged confocal microscopic imaging using the voltage-dependent dye oxonol VI. Imaging analysis showed that fractional fluorescence intensity was clearly decreased in VSMCs from both TgA20 and TgA3 mice at basal conditions (Fig. 13A). The decreased intensities suggested that *Tric-a*-overexpressing VSMCs were deeply hyperpolarized during the resting state (Fig. 13B). We previously prepared the calibration plot representing the relationship between the fluorescence

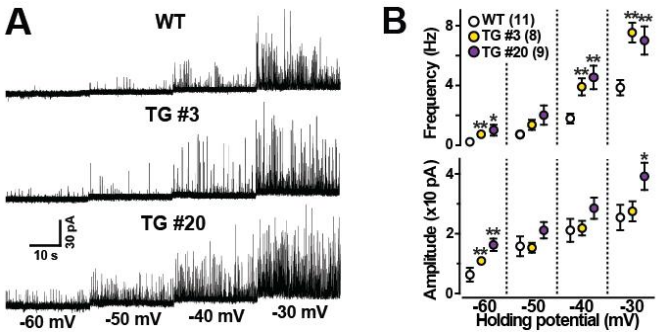

Figure 11. Facilitated STOCs in *Tric-a*-overexpressing VSMCs.

The membrane potential of single VSMCs was controlled by the whole-cell patch-clamp technique using the STOC pipette to monitor membrane currents. Representative STOC recording data are illustrated in (*A*). The data for STOC frequency and amplitude are summarized in (*B*). The data represent the mean ± SEM, and the numbers of cells examined from at least 3 mice are shown in parentheses. Significant differences between the genotypes are indicated by asterisks (**p*<0.05, ***p*<0.01 by *t*-test).

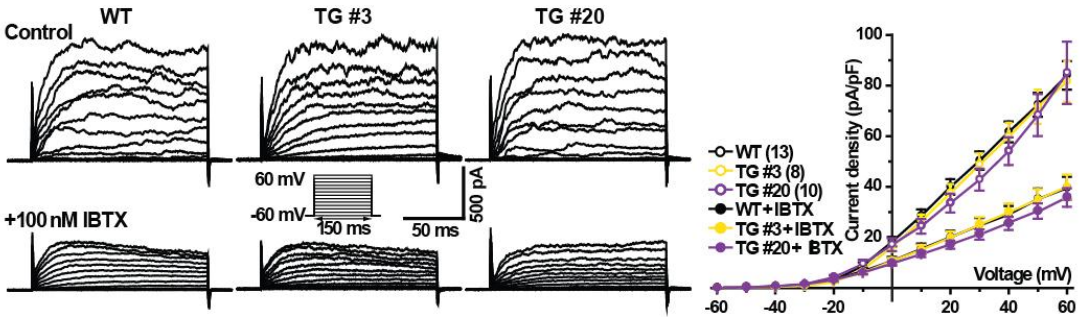

Figure 12. Total K^+ currents in *Tric-a*-overexpressing VSMCs.

Cell-surface K^+ channel density in VSMCs. Single VSMCs were examined using the BK pipette solution and depolarized from a holding potential of -60 mV to test potentials in 10 mV steps. Representative current traces before and after iberiotoxin (IBTX) application are shown. Currents evoked at test potentials were normalized to membrane capacitance to yield the current density, and the data obtained are summarized as current-voltage relationship curves in the right graph. We detected no altered IBTX-sensitive or IBTX-insensitive currents in *Tric-a*-overexpressing VSMCs.

intensity and membrane potential using the reported resting potential of -59.9 mV in wild-type VSMCs (15, 34). The calibration plot estimated that the resting membrane potentials of TgA3, TgA20 and *Tric-a*-knockout VSMCs were -63.6, -63.9 and -54.6 mV, respectively. The estimated potentials agreed closely with actual measurement values from direct monitoring using high-resistance microcapillary electrodes; the detected resting potentials of wild-type, TgA20 and *Tric-a*-knockout VSMCs were -59.4 ± 0.6, -64.8 ± 1.0 and -53.7 ± 0.7 mV, respectively (Fig. 14B). Moreover, from oxonol VI imaging, enlarged intensity shifts were evoked by iberiotoxin in VSMCs from the transgenic mice (Fig. 13C). The enhanced responses directly reflected the hyperactivation of BK channels at resting conditions in *Tric-a*-overexpressing VSMCs. However, while being exposed to iberiotoxin, similar fractional intensities were observed in wild-type and *Tric-a*-overexpressing VSMCs. Because many channels and transporters, in addition to BK channels, contribute to generating resting potential, the iberiotoxin-induced realignment of resting intensities suggested that the components other than BK channels functioned normally on the cell-surface of *Tric-a*-overexpressing VSMCs. In summary, these results suggest that specific hyperactivation of BK channels lowered resting membrane potential in VSMCs from the transgenic mice.

Altered Ca^{2+} Handling in *Tric-a*-Overexpressing VSMCs

Of the excitable cell types, SMCs have relatively shallow resting membrane potentials. In VSMCs at basal conditions, L-type voltage-gated Ca^{2+} channels generate persistent

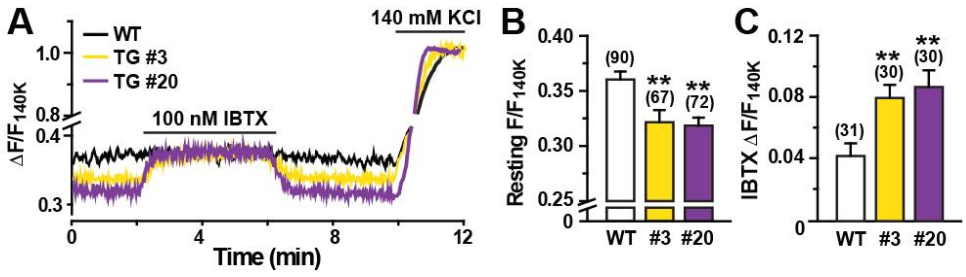

Figure 13. Decreased resting membrane potential in *Tric-a*-overexpressing VSMCs.

Single VSMCs were examined by confocal microscopic imaging using the voltage-dependent dye oxonol VI. Cellular fluorescence intensities were normalized to the maximum value to yield the fractional intensity (F/F_{140K}). (*A*) Representative imaging data. (*B*) The summarized data of the resting intensity. (*C*) The summarized data of the intensity shift by iberiotoxin (IBTX). The data represent the mean ± SEM, and the numbers of cells examined from at least 3 mice are shown in parentheses. Significant differences between the genotypes are indicated by asterisks (**p<0.01 by *t*-test).

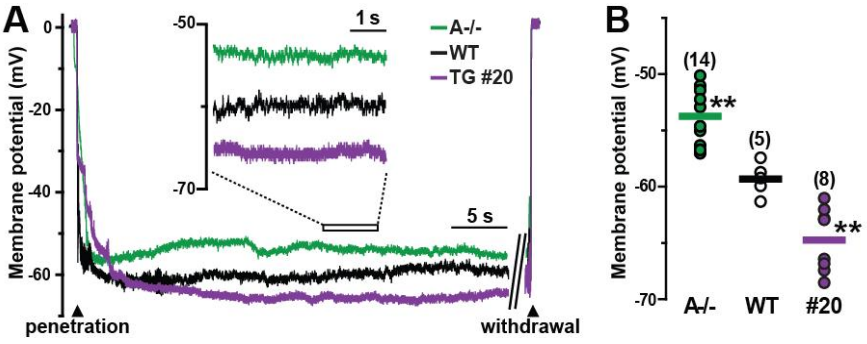

Figure 14. Direct membrane potential recordings using high-resistance microelectrodes in VSMCs.

(*A*) shows representative recording traces from the *Tric-a*-transgenic (TgA20), *Tric-a*-knockout and wild-type VSMCs. The recording data from six TgA20 mice, five *Tric-a*-knockout and five wild-type mice are summarized in (*B*). The data represent the mean ± SEM, and the numbers of cells examined are shown in parentheses. Significant differences are indicated by asterisks (**p<0.01 by *t*-test).

Ca^{2+} influx and maintain both resting $[Ca^{2+}]_i$ and intrinsic tonus (3, 4). We examined cellular Ca^{2+} handling in VSMCs from the transgenic mice and found several abnormal features. First, our ratiometric Fura-PE3 imaging detected that resting $[Ca^{2+}]_i$ was markedly decreased in VSMCs from the transgenic mice (Fig. 15A and B). In accordance with the detected membrane potentials, TgA20 cells exhibited slightly lower $[Ca^{2+}]_i$ than TgA3 cells. In a Ca^{2+}-free extracellular solution, similar resting $[Ca^{2+}]_i$ levels were observed in wild-type and *Tric-a*-overexpressing VSMCs. Moreover, the downward-adjusted resting $[Ca^{2+}]_i$ was clearly rescued by the L-type Ca^{2+} channel inhibitor verapamil and the activator BayK8644 in *Tric-a*-overexpressing VSMCs (Fig. 15C). Therefore, L-type Ca^{2+} channels were likely inactivated at basal conditions, and resting $[Ca^{2+}]_i$ was thus decreased in *Tric-a*-overexpressing VSMCs.

VSMCs contain both IP_3- and caffeine-sensitive stores, and they are functionally interconnected (3, 4). The SR/ER Ca^{2+}-pump inhibitor cyclopiazonic acid (CPA) causes Ca^{2+} leakage from both stores, and the total stored Ca^{2+} contents can be estimated from CPA-induced responses. CPA-induced Ca^{2+} depletion from intracellular stores generally triggers store-operated Ca^{2+} entry (SOCE) (35). VSMCs from the transgenic mice exhibited normal CPA-induced and SOCE responses (Fig. 15D and E). However, *Tric-a*-overexpressing VSMCs showed weak IP_3R-mediated Ca^{2+} release in response to the α-adrenoceptor agonist phenylephrine (PE) (Fig. 15F and G). I also observed that PE-induced responses were diminished after normal caffeine-evoked transients in *Tric-a*-overexpressing VSMCs (Fig. 16). Furthermore, in response to sequential applications of PE and caffeine under Ca^{2+}-free conditions, *Tric-a*-overexpressing

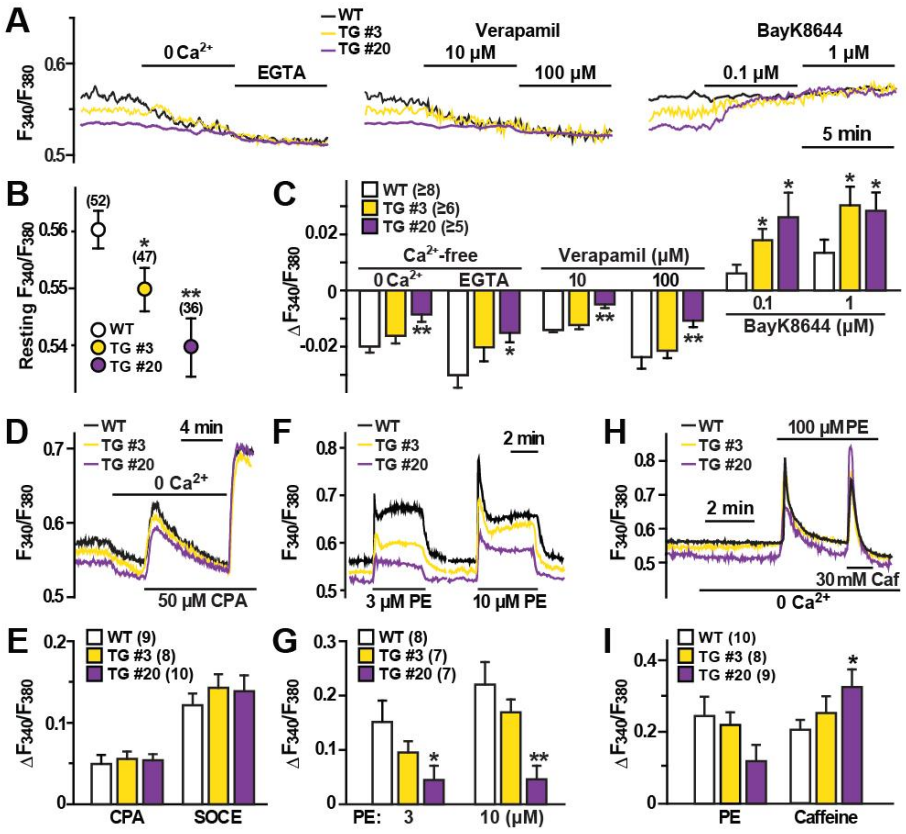

Figure 15. Abnormal Ca^{2+} handling in *Tric-a*-overexpressing VSMCs.

VSMC segments were examined by Fura-PE3 Ca^{2+} imaging. The change in $[Ca^{2+}]_i$ was expressed as ratio of the fluorescence intensity (F_{340}/F_{380}). (*A-C*) Decreased resting $[Ca^{2+}]_i$ in *Tric-a*-overexpressing VSMCs. (*A*) Representative traces under normal conditions and responses to Ca^{2+} removal and L-type Ca^{2+} channel modulators are illustrated. Resting $[Ca^{2+}]_i$ data are summarized in (*B*), and $[Ca^{2+}]_i$ responses are analyzed in (*C*). (*D-E*) Normal Ca^{2+} store contents in *Tric-a*-overexpressing VSMCs. Representative CPA-induced responses are shown in (*D*), and the data are summarized in (*E*). (*F-G*) Impaired IP_3-mediated Ca^{2+} release in *Tric-a*-overexpressing VSMCs. Representative phenylephrine (PE)-induced responses are shown in (*F*), and the data are summarized in (*G*). (*H-I*) Altered Ca^{2+} distribution to store compartments in *Tric-a*-overexpressing VSMCs. Sequential responses to PE and caffeine (Caf) under Ca^{2+}-free conditions are shown in (*H*), and the data are summarized in (*I*). The data represent the mean ± SEM, and the numbers of mice examined are shown in parentheses. Significant differences between the genotypes are indicated by asterisks (*****p<0.05, ******p<0.01 by *t*-test).

VSMCs exhibited poor IP_3R-mediated transients immediately followed by enhanced RyR-mediated transients (Fig. 15H and I). It is unlikely that poor PE-induced transients were due to compromised phosphoinositide turnover signaling because RT-PCR analysis suggested normal expression of major components of adrenoceptor-mediated signaling in *Tric-a*-overexpressing VSMCs (Fig. 10). Therefore, in addition to facilitating Ca^{2+} spark generation as described above, *Tric-a* overexpression appeared to affect IP_3-sensitive stores in VSMCs.

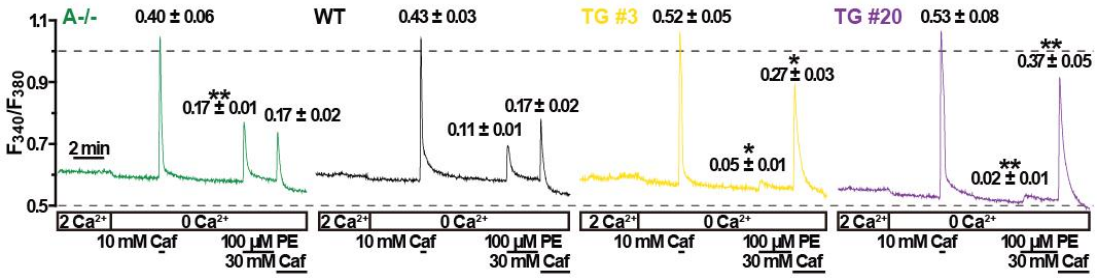

Figure 16. Altered intracellular Ca^{2+} stores in *Tric-a*-overexpressing VSMCs.
Representative sequential responses to caffeine (Caf, 10 or 30 mM) and phenylephrine (PE, 100 μM) under Ca^{2+}-free conditions in VSMCs from the *Tric-a*-transgenic, *Tric-a*-knockout and wild-type mice. Peak amplitudes ($\Delta F_{340}/F_{380}$) represent the mean ± SEM. Significant differences between the mutant and wild-type VSMCs are indicated by asterisks (*****p<0.05, ******p<0.01 by *t*-test).

Discussion

Single-channel recording in planar lipid bilayers demonstrated that purified TRIC-A and TRIC-B proteins form monovalent cation-specific channels (12-14). Therefore, TRIC channel subtypes likely function as SR/ER K^+ channels under intracellular conditions. Although TRIC channels exhibit marked voltage dependence, they are likely to contribute to persistent K^+ flux when membrane potential and osmotic pressure fluctuate in the SR/ER (11). In our previous study, *Tric-a*-knockout mice displayed high vascular tonus and developed hypertension because the hyperpolarization signaling triggered by Ca^{2+} sparks was compromised in the knockout VSMCs (15). In the present study, as a polar opposite of the TRIC-A-null model, SMC-specific *Tric-a*-transgenic mice developed hypotension, and Ca^{2+} spark generation was facilitated in *Tric-a*-overexpressing VSMCs. Therefore, our group reasonably conclude that TRIC-A channels support RyR-mediated Ca^{2+} spark generation and contribute to setting the basal tonus in VSMCs. From a biophysical point of view, the density-dependent contribution of TRIC-A channels to Ca^{2+} spark generation can be explained by an oversimplified scheme (Fig. 17). Several lines of evidence indicate that RyR subtypes are nonselective cation channels equipped with large-diameter pores and can bidirectionally conduct Ca^{2+} and K^+ (36). The model presented here tentatively assumes that only K^+ provided by TRIC-A or RyR channels acts as a counter-ion for stabilizing SR membrane potential during Ca^{2+} release. In wild-type VSMCs, both TRIC-A and

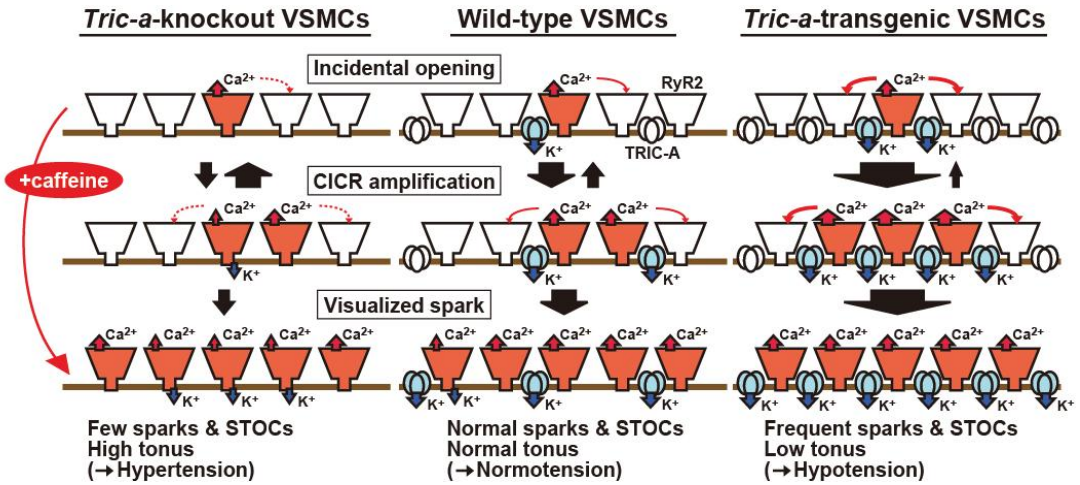

Figure 17. Hypothetical scheme for TRIC-A channel-mediated regulation of Ca^{2+} spark generation in VSMCs.

Although the ionic fluxes are largely unknown in intracellular stores, this over-simplified model for caffeine-sensitive stores assumes that only TRIC-A and RyR2 channels carry counter-K^+ currents coupled with Ca^{2+} sparks in VSMCs. The colored channels contribute to net ionic fluxes across the SR membrane. Additionally, two undetectable Ca^{2+} release processes are proposed during the growth to visualized Ca^{2+} sparks (lower row); initial Ca^{2+} release by incidental RyR opening primarily depends upon the Ca^{2+} gradient between the SR and the cytoplasm (upper row), whereas the subsequent signal amplification mediated by Ca^{2+}-induced Ca^{2+} release (CICR) is likely to require counter-K^+ currents for neutralizing the membrane potential generated by Ca^{2+} release (middle row). *Tric-a*-knockout and *Tric-a*-overexpressing VSMCs displayed a decrease or an excess of Ca^{2+} sparks, respectively. The observations suggest that Ca^{2+} spark generation depends critically upon TRIC-A-mediated K^+ current density in the SR; K^+ currents are likely to stabilize the SR membrane potential and thus effectively maintain the CICR-mediated amplification for Ca^{2+} spark generation. Because RyR subtypes are poorly selective cation channels that can conduct K^+ and Ca^{2+} bidirectionally, they may be responsible for contributing to the overall counter-ion current. Presumably, any counter-ion current via RyRs becomes important for the Ca^{2+} sparks and caffeine-induced transients observed in *Tric-a*-knockout muscle cell types.

RyR channels may conduct counter-K^+ to support Ca^{2+} release. However, the SR K^+ currents are likely insufficient to stabilize membrane potential during vital Ca^{2+} release, and many events of incidental RyR opening may fail to grow to the Ca^{2+} sparks visualized in Ca^{2+}-imaging analysis. Even lower SR K^+ currents are proposed for *Tric-a*-knockout VSMCs, and thus, the growth to detectable Ca^{2+} sparks is further attenuated by the TRIC-A-null conditions. In contrast, in *Tric-a*-overexpressing VSMCs, enhanced SR K^+ currents may no longer attenuate the growth of Ca^{2+} sparks. Additionally, the excess K^+ currents mediated by overexpressed TRIC-A channels may persistently prevent negative-shifting of the membrane potential toward the Ca^{2+} reversal potential and could effectively maintain Ca^{2+} release from partially depleted stores. Such biophysical mechanisms likely underlie the facilitated Ca^{2+} sparks observed in *Tric-a*-overexpressing VSMCs. In the present study, several altered functions linked to the hypotensive phenotype were characterized in *Tric-a*-overexpressing VSMCs (Fig. 18). Excess TRIC-A channels facilitate Ca^{2+} spark (Fig. 9) and STOC generation (Fig. 11) and decrease resting membrane potential in VSMCs (Fig. 13, 14). Under such hyperpolarized conditions, L-type Ca^{2+} channels are relatively inactivated, and resting $[Ca^{2+}]_i$ is suppressed in *Tric-a*-overexpressing VSMCs (Fig. 15). Decreased $[Ca^{2+}]_i$ in VSMCs likely reduces the intrinsic tonus of resistance arteries, leading to hypotension in the *Tric-a*-transgenic mice (Fig. 5).

VSMCs possess both caffeine- and IP_3-sensitive stores and contain both TRIC-A and TRIC-B channels with similar estimated expression levels (15). In accordance with previous studies (37-39), our Ca^{2+} imaging also detected that caffeine-induced responses

were larger than agonist-induced responses in wild-type VSMCs from mesenteric arteries (Fig. 15H). In addition to the altered features directly linked to hypotension, *Tric-a*-overexpressing VSMCs exhibited an unexplainable abnormality in SR Ca^{2+} handling; PE-induced Ca^{2+} release was attenuated despite unchanged total Ca^{2+} content in the SR (Fig. 15D). In contrast, *Tric-a*-knockout VSMCs exhibit facilitated PE-induced Ca^{2+} release from the Ca^{2+}-overloaded SR (15). The alterations in PE-induced response appear to display a mirror image between *Tric-a*-overexpressing and knockout VSMCs (Fig. 16). Low Ca^{2+} contents of IP_3-sensitive stores may contribute to impaired PE-induced Ca^{2+} release in *Tric-a*-overexpressing cells because the sequential application of PE and caffeine implied poor loading in IP_3-sensitive stores (Fig. 15H). In this case, overexpressed TRIC-A channels may selectively gather Ca^{2+} into caffeine-sensitive stores to relatively deplete IP_3-sensitive stores in VSMCs. Because IP_3R channels are activated by both high luminal and cytoplasmic Ca^{2+} (1, 38), lowered luminal and cytoplasmic Ca^{2+} levels may synergistically inhibit IP_3R channels in *Tric-a*-overexpressing VSMCs, whereas elevated Ca^{2+} levels on both sides could facilitate IP_3Rs in *Tric-a*-knockout VSMCs. Alternatively, altered PE-induced responses could be explained by differentially modulated IP_3Rs in *Tric-a*-overexpressing and knockout VSMCs. In addition to generating counter-currents favorable to RyR activation, the TRIC-A protein might inhibit IP_3R channels in VSMCs. These postulated inhibitory effects might be enhanced to remarkably depress PE-induced Ca^{2+} release in *Tric-a*-overexpressing VSMCs but might be removed to facilitate PE-evoked responses in *Tric-a*-knockout VSMCs. Furthermore, other molecular mechanisms can also be

hypothesized for the altered PE-induced Ca^{2+} release depending upon TRIC-A contents. To further investigate the mysterious role of TRIC-A channels in IP_3-sensitive stores, physiological measurements of the mutant VSMCs under membrane-permeable "skinned" conditions, together with comprehensive proteomic survey for its binding partners in Ca^{2+} stores, would be required in future studies. From another point of view, it can be presumed that TRIC-A and TRIC-B channels may have distinct subtype-specific roles in SR Ca^{2+} handling. To verify this possibility, *Tric-b*-overexpressing VSMCs, producible with the use of similar transgenic technology, will provide an important model system.

In our clinical study, the *TRIC-A* gene polymorphisms in the Japanese population were associated with both hypertension susceptibility and sensitivity to antihypertensive medications (15). As discussed above, TRIC-A channel density in VSMCs is an important determinant of basal blood pressure at the whole animal level. Therefore, the human hypertensive risk allele is likely associated with relatively low *Tric-a* expression in VSMCs. Hypertension represents a major health problem with an appalling annual toll, and various antihypertensive drugs have been developed. However, hypertension still remains resistant to multiple antihypertensive medications in a considerable number of patients. Although renal sympathetic denervation has recently come into use in patients with malignant hypertension, novel target proteins are still required for creating new medication strategies (40). Our transgenic mice, together with the knockout mice, suggest that TRIC-A channel openers may potentially be drugs with benefits for malignant hypertension.

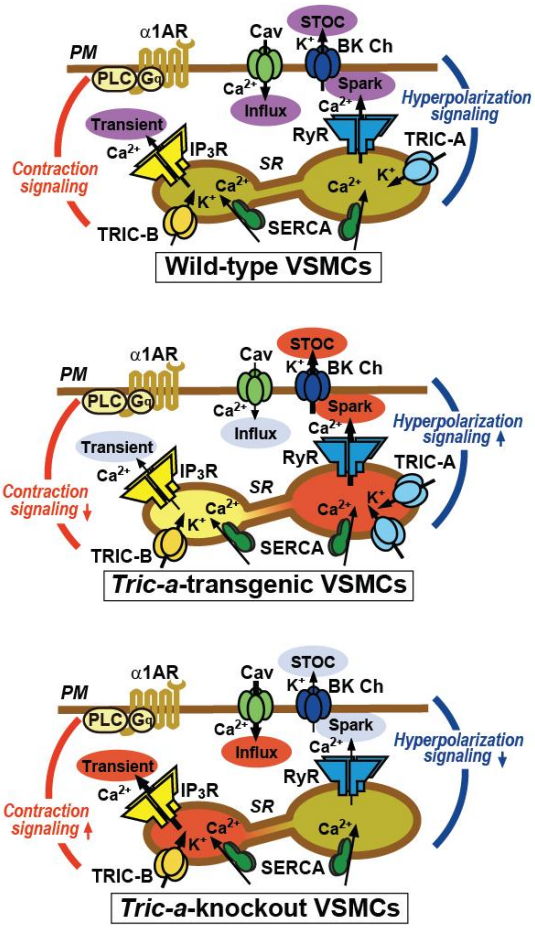

Figure 18. Facilitated hyperpolarization signaling in *Tric-a*-overexpressing VSMCs. *Tric-a* overexpression appears to activate Ca^{2+} spark generation directly, thus facilitating the hyperpolarization signaling produced by functional coupling between RyR and BK channels and decreasing the resting membrane potential in VSMCs. In this situation, L-type Ca^{2+} channels (Cav) are inactivated, and resting $[Ca^{2+}]_i$ is decreased to develop insufficient spontaneous tonus in resistance arteries and hypotension in the transgenic mice. Upon sympathetic stimulation, the α1-adrenoceptor (α1AR), trimeric GTP-binding protein Gq and phospholipase C (PLC) are coordinately activated to trigger IP_3R-mediated Ca^{2+} release. In *Tric-a*-overexpressing VSMCs, IP_3R-mediated Ca^{2+} release is unexpectedly impaired. The poor agonist-induced Ca^{2+} release may be due to partial depletion of IP_3-sensitive stores or TRIC-A-mediated inhibition of IP_3Rs. In contrast, hyperpolarization signaling is impaired, and IP_3-sensitive stores are likely overloaded in *Tric-a*-knockout VSMCs (15).

Summary

An alternative interpretation would be that the overexpression of TRIC-A somehow enhances the activity of RyRs as a result of either a favorable counter ion movement or a direct interaction between RyR and TRIC-A. The enhanced RyR activity would lead to more Ca^{2+} sparks, which would activate BK_{Ca} and STOCs, resulting in membrane hyperpolarization and inactivation of L-type Ca^{2+} channels (thus reduced resting cytosolic Ca^{2+} level).

At the same time, the enhanced RyR activity would tend to reduce the intracellular Ca^{2+} store, which would in turn decrease the activity of the IP_3R via SR luminal Ca^{2+} dependent regulation The reduced IP_3R activity would explain the lack of response to PE. Another alternative interpretation would be that TRIC-A may regulate the activity of RyRs and IP_3Rs in an opposite manner.

In other words, overexpressing TRIC-A enhances the activity of RyRs and suppresses the activity of IP_3Rs. On the contrary, TRIC-A KO suppresses RyRs, but activates IP_3Rs.

Acknowledgment

本論文をまとめるにあたり、終始暖かい激励とご指導、ご鞭撻を頂いた京都大学薬学研究科教授竹島浩教授に謹んで感謝を申し上げます。また、多くの貴重なご指導とご助言を頂いた薬学研究科山崎大樹講師並びに柿澤昌准教授、竹島美幸准教授、山本伸一郎助教に心より感謝を申し上げます。さらに、博士課程在学中、同期の趙成珠、範博、飯田綱規、銭年超、内藤大督、王朝弘及び京都大学薬学研究科生体分子認識学分野の皆様が研究を進めていく上で、大きな励みとなったことをここに記すともに、深く感謝申しあげます。

Ca^{2+} spark 及び微小電極法細胞膜電位測定実験の実施にあたり、ご協力頂いた、名古屋市立大学薬学研究科の今泉祐治教授及び山村寿男准教授、鈴木良明助教他、細胞分子薬効解析学分野の皆様に心より感謝申しあげます。

電子顕微鏡写真の製作実施にあたり、熱心なご協力をいただいた埼玉医科大学駒崎伸二准教授に心より感謝申しあげます。

本研究において、溝部佑希さんの熱心な協力なくしては、実験の実施は不可能であったことを記すとともに、深甚の謝意を表します。

また、研究を進めるにあたり、ご支援、ご協力を頂きながら、ここにお名前を記すことが出来なかった多くの方々に心より感謝申しあげます。

最後に、私が研究活動に専念できるよう終始支えいただきました父母、そして妻に心から感謝いたします。

Publication List

本研究は以下の論文に公表した。

1. Facilitated Hyperpolarization Signaling in Vascular Smooth Muscle-overexpressing TRIC-A Channels

   （平滑筋特異的 TRIC-A 過剰発現マウスにおける過分極シグナルの亢進）

   Shengchen Tao, Daiju Yamazaki, Shinji Komazaki, Chengzhu Zhao, Tsunaki Iida, Sho Kakizawa, Yuji Imaizumi, and Hiroshi Takeshima

   平成 25 年 5 月発行

   The Journal of Biological Chemistry

   第 288 巻 15581 頁～15589 頁に掲載

2. TRIC channel and hypertension

   （TRIC チャネルと高血圧）

   Daiju Yamazaki, Shengchen Tao, Hiroshi Takeshima

   平成 25 年 4 月発行

   Clinical Calcium

   第 23 巻 543 頁～550 頁に掲載

References

1. Bezprozvanny, I., and Ehrlich, B.E. (1995) The inositol 1,4,5-trisphosphate (InsP3) receptor. *J. Membr. Biol.* **145**, 205–216.
2. Meissner, G. (1994) Ryanodine receptor/Ca^{2+} release channels and their regulation by endogenous effectors. *Annu. Rev. Physiol.* **56**, 485–508.
3. Berridge, M.J. (2008) Smooth muscle cell calcium activation mechanisms. *J. Physiol.* **586**, 5047–5061.
4. Wellman, G.C., and Nelson, M.T. (2003) Signaling between SR and plasmalemma in smooth muscle: sparks and the activation of Ca^{2+}-sensitive ion channels. *Cell Calcium* **34**, 211–229.
5. Somlyo, A.V., Gonzalez-Serratos, H.G., Shuman, H., McClellan, G., and Somlyo, A.P. (1981) Calcium release and ionic changes in the sarcoplasmic reticulum of tetanized muscle: an electron-probe study. *J. Cell Biol.* **90**, 577-594.
6. Fink, R.H., and Veigel, C. (1996) Calcium uptake and release modulated by counter-ion conductances in the sarcoplasmic reticulum of skeletal muscle. *Acta Physiol. Scand.* **156**, 387–396.
7. Coronado, R., and Miller, C. (1980) Decamethonium and hexamethonium block K^+ channels of sarcoplasmic reticulum. *Nature* **288**, 495-497.
8. Meissner, G. (1983) Monovalent ion and calcium ion fluxes in sarcoplasmic reticulum. *Mol. Cell. Biochem.* **55**, 65–82.
9. Ide, T., Sakamoto, H., Morita, T., Taguchi, T., and Kasai, M. (1991) Purification of a

Cl^--channel protein of sarcoplasmic reticulum by assaying the channel activity in the planar lipid bilayer system. *Biochem. Biophys. Res. Commun.* **176**, 38-44.

10. Kamp, F., Donoso, P., and Hidalgo, C. (1998) Changes in luminal pH caused by calcium release in sarcoplasmic reticulum vesicles. *Biophys. J.* **74**, 290-296.
11. Venturi, E., Sitsapesan, R., Yamazaki, D., and Takeshima, H. (2013) TRIC channels supporting efficient Ca^{2+} release from intracellular stores. *Pflugers Arch.* **465**, 187-195.
12. Pitt, S.J., Park, K-H., Nishi, M., Urashima, T., Aoki, S., Yamazaki, D., Ma, J., Takeshima, H., and Sitsapesan, R. (2010) Charade of the SR K^+-channel: two ion-channels, TRIC-A and TRIC-B, masquerade as a single K^+-channel. *Biophys. J.* **99**, 417–426.
13. Venturi, E., Matyjaszkiewicz, A., Pitt, S.J., Tsaneva-Atanasova, K., Nishi, M., Yamazaki, D., Takeshima, H., and Sitsapesan, R. (2013) TRIC-B channels display labile gating: evidence from the TRIC-A knockout mouse model. *Pflugers Arch.* **465**, 1135-1148.
14. Yazawa, M., Ferrante, C., Feng, J., Mio, K., Ogura, T., Zhang, M., Lin, P-H., Pan, Z., Komazaki, S., Kato, K., Nishi, M., Zhao, X., Weisleder, N., Sato, C., Ma, J., and Takeshima, H. (2007) TRIC channels are essential for Ca^{2+} handling in intracellular stores. *Nature* **448**, 78–82.
15. Yamazaki, D., Tabara, Y., Kita, S., Hanada, H., Komazaki, S., Naitou, D., Mishima, A., Nishi, M., Yamamura, H., Yamamoto, S., Kakizawa, S., Miyachi, H., Yamamoto, S., Miyata, T., Kawano, Y., Kamide, K., Ogihara, T., Hata, A., Umemura, S., Soma,

M., Takahashi, N., Imaizumi, Y., Miki, T., Iwamoto, T., and Takeshima, H. (2011) TRIC-A channels in vascular smooth muscle contribute to blood pressure maintenance. *Cell Metab.* **14**, 231–241.

16. Zhao, X., Yamazaki, D., Park, K-H., Komazaki, S., Tjondrokoesoemo, A., Nishi, M., Lin, P., Hirata, Y., Brotto, M., Takeshima, H., and Ma, J. (2010) Ca^{2+} overload and sarcoplasmic reticulum instability in tric-a null skeletal muscle. *J. Biol. Chem.* **285**, 37370–37376.
17. Yamazaki, D., Komazaki, S., Nakanishi, H., Mishima, A., Nishi, M., Yazawa, M., Yamazaki, T., Taguchi, R., and Takeshima, H. (2009) Essential role of the TRIC-B channel in Ca^{2+} handling of alveolar epithelial cells and in perinatal lung maturation. *Development* **136**, 2355–2361.
18. Takeshima, H., Komazaki, S., Nishi, M., Iino, M., and Kangawa, K. (2000) Junctophilins: a novel family of junctional membrane complex proteins. *Mol. Cell* **6**, 11-22.
19. Ohi, Y., Yamamura, H., Nagano, N., Ohya, S., Muraki, K., Watanabe, M., and Imaizumi, Y. (2001) Local Ca^{2+} transients and distribution of BK channels and ryanodine receptors in smooth muscle cells of guinea-pig vas deferens and urinary bladder. *J. Physiol.* **534**, 313–326.
20. Iwamoto, T., Kita, S., Zhang, J., Blaustein, M.P., Arai, Y., Yoshida, S., Wakimoto, K., Komuro, I., and Katsuragi, T. (2004) Salt-sensitive hypertension is triggered by Ca^{2+} entry via Na^{+}/Ca^{2+} exchanger type-1 in vascular smooth muscle. *Nat. Med.* **10**, 1193–1199.

21. Hotta, S., Morimura, K., Ohya, S., Muraki, K., Takeshima, H., and Imaizumi, Y. (2007) Ryanodine receptor type 2 deficiency changes excitation-contraction coupling and membrane potential in urinary bladder smooth muscle. *J. Physiol.* **582**, 489-506.

22. Kiyoshi, H., Yamazaki, D., Ohya, S., Kitsukawa, M., Muraki, K., Saito, S.Y., Ohizumi, Y., and Imaizumi, Y. (2006) Molecular and electrophysiological characteristics of K^+ conductance sensitive to acidic pH in aortic smooth muscle cells of WKY and SHR. *Am. J. Physiol. Heart Circ. Physiol.* **291**, H2723-2734.

23. Nakano, Y., Nishihara, T., Sasayama, S., Miwa, T., Kamada, S., and Kakunaga, T. (1991) Transcriptional regulatory elements in the 5' upstream and first intron regions of the human smooth muscle (aortic type) alpha-actin-encoding gene. *Gene* **99**, 285–289.

24. Smith, O.A. (1974) Reflex and central mechanisms involved in the control of the heart and circulation. *Annu. Rev. Physiol.* **36**, 93-123.

25. Pathak, R.K., Luskey, K.L., and Anderson, R.G. (1986) Biogenesis of the crystalloid endoplasmic reticulum in UT-1 cells: evidence that newly formed endoplasmic reticulum emerges from the nuclear envelope. *J. Cell Biol.* **102**, 2158-2168.

26. Snapp, E.L., Hegde, R.S., Francolini, M., Lombardo, F., Colombo, S., Pedrazzini, E., Borgese, N., and Lippincott-Schwartz, J. (2003) Formation of stacked ER cisternae by low affinity protein interactions. *J. Cell Biol.* **163**, 257-269.

27. Tasker, P.N., Michelangei, F., and Nixon, G.F. (1999) Expression and distribution of the type 1 and type 3 inositol 1,4,5-trisphospate receptor in developing vascular

smooth muscle. *Circ. Res.* **84**, 536-542.

28. Vermassen, E., Van Acker, K., Annaert, W.G., Himpens, B., Callewaert, G., Missaen, L., De Smedt, H., and Parys, J.B. (2003) Microtubule-dependent redistribution of the type-1 inositol 1,4,5-trisphosphate receptor in A7r5 smooth muscle cells. *J. Cell Sci.* **116**, 1269-1277.
29. Lesh, R.E., Nixon, G.F., Fleischer, S., Airey, J. A., Somlyo, A.P., and Somlyo, A.V. (1998) Localization of ryanodine receptors in smooth muscle. *Circ. Res.* **82**, 175-185.
30. Moore, E.D., Voigt, T., Kobayashi, Y.M., Isenberg, G., Fay, F.S., Gallitelli, M.F., and Franzini-Armstrong, C. (2004) Organization of Ca^{2+} release units in excitable smooth muscle of the guinea-pig urinary bladder. *Biophys. J.* **87**, 1836-1847.
31. Devine, C.E., Somlyo, A.V., and Somlyo, A.P. (1972) Sarcoplasmic reticulum and excitation-contraction coupling in mammalian smooth muscles. *J. Cell Biol.* **52**, 690-718.
32. Ikemoto, T., Takeshima, H., Iino, M., and Endo, M. (1998) Effect of calmodulin on Ca^{2+}-induced Ca^{2+} release of skeletal muscle from mutant mice expressing either ryanodine receptor type 1 or type 3. *Pflugers Arch.* **437**, 43-48.
33. Takeshima, H., Komazaki, S., Hirose, K., Nishi, M., Noda, T., and Iino, M. (1998) Embryonic lethality and abnormal cardiac myocytes in mice lacking ryanodine receptor type 2. *EMBO J.* **17**, 3309-3316.
34. Koshita, M., Hidaka, K., Ueno, H., Yamamoto, Y., and Suzuki, H. (2007) Properties of acetylcholine-induced hyperpolarization in smooth muscle cells of the mouse

mesenteric artery. *J. Smooth Muscle Res.* **43**, 219–227.

35. Smyth, J.T., Hwang, S.Y., Tomita, T., DeHaven, W.I., Mercer, J.C., and Putney, J.W. (2010) Activation and regulation of store-operated calcium entry. *J. Cell. Mol. Med.* **14**, 2337-2349.
36. Gillespie, D., Chen, H., and Fill, M. (2012) Is ryanodine receptor a calcium or magnesium channel? Roles of K^+ and Mg^{2+} during Ca^{2+} release. *Cell Calcium* **51**, 427-433.
37. Iino, M. (1990) Calcium release mechanisms in smooth muscle. *Jpn. J. Pharmacol.* **54**, 345-354.
38. Iino, M. (2000) Molecular basis of spatio-temporal dynamics in inositol 1,4,5-trisphosphate-mediated Ca^{2+} signalling. *Jpn. J. Pharmacol.* **82**, 15-20.
39. Bolton, T.B., Prestwich, S.A., Zholos, A.V., and Gordienko, D.V. (1999) Excitation-contraction coupling in gastrointestinal and other smooth muscles. *Annu. Rev. Physiol.* **61**, 85-115.
40. Laurent, S., Schlaich, M., and Esler, M. (2012) New drugs, procedures, and devices for hypertension. *Lancet* **380**, 591-600.